doi.org/10.36721/PJPS.2026.39.9.241.1

Research on mechanism of exosome derived from EOC on promoting BMSCs and its autocrine effect in micro-environment through activating the VEGF-A/MAPK/ERK pathway

Shuhan Lv[1], Yong Liang[1] and Chengbin Wang[2]*

[1]Department of First Clinical Medical College, Guizhou University of Traditional Chinese Medicine, Guiyang, Guizhou, 550025, China
[2]Department of Second Clinical Medical College, Guizhou University of Traditional Chinese Medicine, Guiyang, Guizhou, 550025, China

Abstract: **Background**: Tumor-derived exosomes mediate intercellular communication in the tumor microenvironment. Epithelial ovarian cancer (EOC) cells secrete exosomes that may regulate bone marrow mesenchymal stem cells (BMSCs), but the underlying mechanisms remain unclear. **Objectives**: This study aimed to investigate whether EOC-derived exosomes regulate BMSCs through the Vascular Endothelial Growth Factor A(VEGF-A)/Mitogen-Activated Protein Kinase(MAPK)/Extracellular Signal-Regulated Kinase(ERK) signaling pathway and to determine the functional consequences of this interaction. **Methods**: EOC-derived exosomes (EOC-Exos) were isolated by ultracentrifugation and characterized by transmission electron microscopy, nanoparticle tracking analysis and Western blot. BMSCs were identified by flow cytometry. BMSCs were divided into control, EOC-Exos and EOC-Exos + ERK inhibitor (U0126) groups. Cell cycle distribution was analyzed by flow cytometry. VEGF-A and MAPK/ERK expression were detected by immunofluorescence and Western blot. VEGF secretion was measured by enzyme-linked immunosorbent assay (ELISA) and VEGF mRNA expression was detected by reverse transcription-polymerase chain reaction (RT-PCR). **Results**: EOC-Exos exhibited a typical cup-shaped morphology, ranged from 30 to 150 nm in size and expressed CD9, CD63 and TSG101. BMSCs highly expressed CD90, CD73 and CD105, with low CD45 and CD34. EOC-Exos treatment significantly decreased the proportion of cells in G0/G1 phase (P=0.007) and increased that in S phase (P<0.001), indicating accelerated cell cycle progression. EOC-Exos time-dependently upregulated VEGF-A protein (P<0.05) and ERK phosphorylation (P<0.001). ERK inhibitor U0126 significantly attenuated EOC-Exos-induced VEGF upregulation (P<0.01), VEGF mRNA expression (P<0.01) and S phase increase (P<0.01). **Conclusion**: EOC-derived exosomes activate the MAPK/ERK pathway in BMSCs, upregulating VEGF transcription and secretion and accelerating cell cycle progression. ERK inhibition reverses these effects, demonstrating the critical role of this pathway in tumor-stroma interactions.

Keywords: Autocrine effect; BMSCs; Exosome derived from EOC; MAPK/ERK; Micro-environment; VEGF-A

Submitted on 04-02-2026 – Revised on 09-03-2026 – Accepted on 25-03-2026

INTRODUCTION

Bone marrow mesenchymal stem cells (BMSCs) are one of the important pluripotent stem cells in the body, possessing multilineage differentiation potential and tissue tropism (Liu *et al*., 2022). Due to their ease of acquisition and expansion, they are often used as seed cells in tissue engineering research. Through different interventions, BMSCs can be induced to differentiate into specific directions. Studying the genetic factors and related signaling pathways on the surface of BMSCs, observing their differentiation differences and analyzing their mechanisms of action in tissue engineering, pathological processes and related diseases are expected to provide novel targets and approaches for disease treatment.

Exosomes are important substances secreted by living cells that mediate intercellular information transfer. They are small vesicles formed through the endocytic pathway, carrying various biological information molecules such as proteins, messenger RNA (mRNA) and microRNA (miRNA). Exosomes complete signal transduction between cells by fusing with the target cell membrane or releasing their contents into the target cell, thereby affecting the physiological or pathological state of the recipient cell (Elieh-Ali-Komi *et al*., 2025). The components carried by exosomes from different cell sources are complex and varied, which not only helps maintain the homeostasis of the cellular environment but also extensively participates in various physiological and pathological processes of the body (Gangadaran *et al*., 2023). The cellular microenvironment is the specialized environment required for cell growth and proliferation, composed of various cells and the extracellular matrix. A normal cellular microenvironment maintains the dynamic balance of cell growth. Once this balance is disrupted, it may lead to malignant cell proliferation and affect normal cellular biological functions (Iqbal *et al*., 2024). The activation of vascular endothelial cells is crucial during tumor proliferation. Tumor cell proliferation is often accompanied by the formation of new blood vessels (Lei *et*

**Corresponding author:* e-mail: wcbjn007@163.com

al., 2024). New blood vessels not only transport large amounts of oxygen and nutrients for tumor growth but also help tumors discharge metabolic waste, while providing channels for the distant metastasis of tumor cells (Leong *et al*., 2022). Vascular endothelial growth factor (VEGF) is a key factor in the process of endothelial cell formation of new blood vessels. It can bind to vascular endothelial growth factor receptor (VEGFR) through paracrine action, activating downstream signaling pathways and inducing cell proliferation (Kimura *et al*., 2022). During tumor cell proliferation, endothelial cells not only show high expression but also possess autocrine function (Doppelt-Flikshtain *et al*., 2023). Endothelial cells can produce autocrine substances during mitosis, which can increase vascular permeability and accelerate the release of tumor growth factors (Chen *et al*., 2023), thereby promoting cell division and proliferation (Liang *et al*., 2024). The mitogen-activated protein kinase (MAPK)/extracellular signal-regulated kinase (ERK) signaling pathway is a classic mediator of cell mitosis (Murase *et al*., 2024). It regulates both cell cycle progression and apoptosis. Activating this pathway can promote the transfer of related genes from the cytoplasm to the nucleus, thereby accelerating the cell cycle and inhibiting the expression of apoptosis-related genes (Wu *et al*., 2025). In tumor cells, this pathway shows a clear trend of activation. This study aims to investigate the potential mechanism by which exosomes derived from epithelial ovarian cancer (EOC) promote BMSC proliferation and regulate their autocrine function in the microenvironment through activating the vascular endothelial growth factor A (VEGF-A)/MAPK/ERK signaling pathway, hoping to provide new ideas for the treatment of EOC.

MATERIALS AND METHODS

Experimental reagents and instruments

Human EOC cell line and human BMSCs (Cell Bank of the Chinese Academy of Sciences Typical Culture Preservation Committee); Dulbecco's modified eagle medium (DMEM), fetal bovine serum (FBS), penicillin-streptomycin (Gibco, USA); ERK inhibitor U0126 (Selleck Chemicals, USA); bicinchoninic acid (BCA) protein quantification kit, radioimmunoprecipitation assay (RIPA) lysis buffer (Beyotime Biotechnology, Shanghai, China); rabbit anti-human VEGF-A polyclonal antibody (Cat# ab46154); CD90-phycoerythrin (PE) (Cat# ab225), CD45-allophycocyanin (APC) (Cat# ab22147), CD73-PE (Cat# ab157335), CD105-APC (Cat# ab221675), Exosome markers CD9 antibody (Cat# ab92726), CD63 antibody (Cat# ab217345), TSG101 antibody (Cat# ab125011); horseradish peroxidase (HRP)-labeled goat anti-rabbit secondary antibody (Cat# SA00001-2), FITC-labeled fluorescent secondary antibody (Cat# SA00003-11) (Boster Biological Technology, Wuhan, China); Human VEGF ELISA kit (Cat# DVE00, R&D Systems, USA); Reverse transcription and real-time polymerase chain reaction (PCR) kits (Cat# K1622, 4367659, Thermo Fisher Scientific, USA); Exosome extraction related consumables (0.22 μm filter, ultracentrifuge tubes, Beckman Coulter, USA); enhanced chemiluminescence (ECL) reagent (Cat# WBKLS0500, Millipore, USA). Rabbit anti-human p-ERK1/2 (Thr202/Tyr204) monoclonal antibody (CST, USA), Rabbit anti-human total ERK1/2 antibody (CST, USA). MAPK/ERK pathway specific inhibitor U0126 (Selleck Chemicals, USA), dissolved in dimethyl sulfoxide (DMSO).

Main instruments: CO2 incubator (HERAcell 150i, Thermo, USA), Ultracentrifuge (Optima XPN-100, Beckman Coulter, USA, SW 41 Ti rotor), TEM (H-7650, Hitachi, Japan), NTA analyzer (ZetaView, Particle Metrix, Germany), Flow cytometer (FACSCanto II, BD, USA), Real-time PCR system (ABI 7500, Applied Biosystems, USA), Chemiluminescence imaging system (ChemiDoc XRS+, Bio-Rad, USA), Microplate reader (Multiskan FC, Thermo, USA).

Extraction and identification of EOC-derived exosomes

Exosomes secreted by EOC cells were extracted by differential ultracentrifugation combined with density gradient centrifugation. The supernatant of EOC cells cultured to the 3rd passage was collected and centrifuged at 4°C according to the following steps (using a fixed-angle rotor, rotor radius r_max=8.4 cm): (1) 300 rpm for 10 min, pellet was discarded to remove cells; (2) 2000 rpm for 30 min, pellet was discarded to remove dead cells and debris; (3) 10,000 rpm for 30 min, pellet was discarded to remove larger cell vesicles; (4) Supernatant was collected, filtered through a 0.22 μm filter, then ultracentrifuged at 100,000 rpm for 70 min (SW 41 Ti rotor) to discard supernatant, pellet was resuspended in pre-cooled phosphate-buffered saline (PBS); (5) The resuspended liquid was placed onto a 30% sucrose cushion, centrifuged at 100,000 rpm for 75 min, collect the sucrose cushion and exosome-enriched layer; (6) Diluted with a large amount of PBS, then ultracentrifuge again at 100,000 rpm for 70 min, the resulting pellet was the purified exosomes. Finally, the exosome pellet was resuspended in 100-200 μL pre-cooled PBS to determine protein concentration using the BCA method and was stored at -80°C until use.

Exosome identification: (1) Morphological identification: TEM was used for negative staining of nanovesicle morphology. First, a copper grid was placed on a drop of purified nanovesicle suspension. Next, the grid was placed on a drop of 3% glutaraldehyde. Subsequently, the grid was transferred to a drop of water to remove residual fixative and this process was repeated ten times. Finally, the nanovesicles on the grid were stained with 4% uranyl acetate. Then, excess liquid was removed with filter paper. The morphology of the nanovesicles was observed using TEM. (2) Particle size analysis: An appropriate amount of exosome suspension was diluted with sterile PBS followed

by analysis using an NTA analyzer. Set the detection temperature to 25°C and repeat the acquisition for each sample 3 times for 60 seconds each. Analyze the particle size distribution and particle concentration of exosomes using NTA software. (3) Marker protein identification: Extract total exosome protein and determine protein concentration using the BCA protein quantification kit. Take equal amounts of protein (20 μg/lane) for 12% sodium dodecyl sulfate-polyacrylamide gel electrophoresis (SDS-PAGE) (stacking gel at 80 V, separating gel at 120 V). After electrophoresis, transfer the protein to a polyvinylidene fluoride (PVDF) membrane (300 mA, 90 min). Block with Tris-buffered saline with Tween 20 (TBST) containing 5% skim milk for 2 hours at room temperature. Add primary antibodies: rabbit anti-human CD9 (1:1000 dilution), rabbit anti-human CD63 (1:1000 dilution) and rabbit anti-human TSG101 (1:1000 dilution), incubate overnight at 4°C. The next day, wash the membrane 3 times with TBST for 10 minutes each. Add HRP-labeled goat anti-rabbit secondary antibody (1:5000 dilution), incubate for 2 hours at room temperature. After washing 3 times with TBST, develop using ECL reagent and capture images with a gel imaging system.

Culture, identification and grouping of BMSCs

Human BMSCs cell line was purchased from the Cell Bank of the Chinese Academy of Sciences. Cells were cultured in DMEM containing 10% FBS and 1% penicillin-streptomycin in a 37°C, 5% CO_2 incubator. When cells reached 80%-90% confluence, they were digested with 0.25% trypsin and sub cultured at a 1:3 ratio. BMSCs at the 3rd passage (P3) in good growth condition were used for subsequent experiments.

Surface markers of P3 BMSCs were identified by FCM. Cells were collected, washed twice with PBS, adjusted to a density of 1×10^6 cells/mL, aliquoted into flow cytometry tubes (100 μL per tube). Antibodies were added: CD44-FITC (5 μL/tube), CD90-PE (5 μL/tube), CD73-PE (5 μL/tube), CD105-APC (5 μL/tube), as well as hematopoietic stem cell markers CD45-APC (5 μL/tube) and CD34-FITC (5 μL/tube). Isotype controls were also set up. Incubate protected from light at room temperature for 30 min. Wash twice with PBS, resuspend cells in 500 μL PBS and detect the positive expression rate of cell surface markers using a flow cytometer, collecting 10,000 cells per sample.

P3 BMSCs were divided into the following three groups, with 3 replicate wells per group and the experiment was repeated independently 3 times: (1) Control group: Routine culture, add an equal volume of PBS as a blank control. (2) EOC-Exos group: Add EOC-Exos to the culture medium at a final concentration of 200 μg/mL for intervention. (3) EOC-Exos + ERK inhibitor group: Pre-treat cells with the ERK pathway-specific inhibitor U0126 (dissolved in DMSO, final concentration 10 μmol/L) for 1 hour, then add the same dose (200 μg/mL) of EOC-Exos for co-culture. (4) DMSO solvent control group: Add an equal volume of DMSO (final concentration <0.1%) to exclude the effect of the solvent on cell viability.

Cell cycle analysis

After 24 h of corresponding intervention culture, BMSCs from each group were collected and washed twice with pre-cooled PBS. Add pre-cooled 70% ethanol and fix overnight at 4°C. The next day, wash twice with PBS to remove ethanol, add propidium iodide (PI, 50 μg/mL) staining solution containing RNase A (50 μg/mL) and incubate protected from light at room temperature for 30 min. Detect cell cycle distribution using a flow cytometer with excitation wavelength 488 nm and emission wavelength 585 nm, collecting 20,000 cells per sample. Analyze the proportions of cells in G0/G1, S and G2/M phases using ModFit LT 5.0 software (Yang *et al.,* 2020).

Immunofluorescence staining for VEGF-A and total MAPK/ERK distribution

BMSCs were seeded in 24-well plates containing cell slides (density 2×10^4 cells/well), cultured for 24 h and then treated according to grouping. After 24 h of intervention, discard the culture medium, wash 3 times with PBS, fix cells with 4% paraformaldehyde for 20 min at room temperature, permeabilize with 0.5% Triton X-100 for 10 min and block with 5% bovine serum albumin (BSA) for 1 h at room temperature. Then add primary antibodies (rabbit anti-human VEGF-A, 1:200; rabbit anti-human total MAPK/ERK1/2, 1:200) and incubate overnight at 4°C. After washing 3 times with PBS (5 min each), add FITC-labeled fluorescent secondary antibody (1:500), incubate protected from light for 1 h at room temperature. Wash 3 times with PBS, counterstain nuclei with 4',6-diamidino-2-phenylindole (DAPI, 1 μg/mL) for 5 min. Finally, mount with anti-fade mounting medium, observe and photograph under a fluorescence microscope (excitation wavelength 488 nm, emission wavelength 520 nm). Randomly select 5 fields of view per slide for image acquisition.

Western blot for protein expression

Cells from each group were collected at 24, 48 and 72 h post-intervention, lysed on ice for 30 min using RIPA lysis buffer containing protease and phosphatase inhibitors and centrifuged at 4°C, 12,000×g for 15 min to extract total protein. Protein concentration was determined by BCA method using BSA as a standard to generate a standard curve. Equal amounts of protein (30 μg) were mixed with 5× loading buffer and denatured by boiling at 100°C for 5 min. Perform 10% SDS-PAGE gel electrophoresis (stacking gel 80 V, 30 min; separating gel 120 V, 60 min), then transfer to a PVDF membrane (300 mA, 90 min). After blocking with 5% skim milk (in TBST) for 1 h at room temperature, add corresponding primary antibodies: VEGF-A (1:1000), total MAPK/ERK1/2 (1:2000), p-MAPK/ERK1/2 (p-ERK1/2, 1:1000) and internal control β-actin (1:5000), incubate overnight at 4°C. The next day, wash 3 times with TBST (10 min each), add HRP-labeled

secondary antibody (1:5000), incubate for 1 h at room temperature. After washing 3 times with TBST, develop using ECL method. Analyze band grayscale values using Image J 1.53 software and express relative protein expression as the ratio of target protein to internal control β-actin grayscale value. To detect the activation status of the ERK pathway, rabbit anti-human p-ERK1/2 antibody (1:2000) was used to detect p-ERK expression level and rabbit anti-human total ERK1/2 antibody (1:2000) was used to detect total ERK expression level. The activation level of the ERK pathway was expressed as the p-ERK/total ERK ratio. To verify the inhibitory effect of the ERK inhibitor, the expression level of p-ERK1/2 was detected in the EOC-Exos + ERK inhibitor group and compared with the control group and EOC-Exos group.

ELISA for VEGF content in cell supernatant

BMSCs from each group were seeded in 24-well plates at a density of 5×10^4 cells/well. After 24 h of corresponding intervention culture, collect the cell culture supernatant, centrifuge at 4°C, 1000 rpm for 10 min to remove cell debris. Operate according to the human VEGF ELISA kit instructions: add 50 μL of Assay Diluent to each well, then add 50 μL of standard or sample, incubate for 2 h at room temperature. Wash 4 times, add 200 μL of VEGF Conjugate, incubate for 2 h at room temperature. Wash 4 times, add 200 μL of Substrate Solution, incubate protected from light for 30 min at room temperature. Add 50 μL of Stop Solution, measure the absorbance at 450 nm wavelength using a microplate reader within 30 min, while setting 540 nm or 570 nm as the correction wavelength. Calculate the VEGF concentration (pg/mL) in the supernatant based on the standard curve. Set up 3 replicate wells for each sample.

Real-time fluorescence quantitative PCR for VEGF mRNA expression

Total RNA was extracted from BMSCs in each group using the TRIzol method. After washing cells with PBS, add 1 mL TRIzol reagent per well, lyse for 5 min at room temperature, transfer to RNase-free EP tubes. Add 200 μL chloroform, shake vigorously for 15 s, let stand for 3 min at room temperature, centrifuge at 4°C, 12,000×g for 15 min. Aspirate the upper aqueous phase, add an equal volume of isopropanol, let stand for 10 min at room temperature, centrifuge at 4°C, 12,000 rpm for 10 min. Discard supernatant, wash the pellet twice with 75% ethanol, dry at room temperature and dissolve in 20 μL diethyl pyrocarbonate (DEPC) water. Determine RNA purity (A260/A280 ratio between 1.8-2.0) and concentration using a spectrophotometer. Take 1 μg total RNA and synthesize complementary DNA (cDNA) by reverse transcription according to the reverse transcription kit instructions (reaction system 20 μL: RNA 1 μg, random primer 1 μL, deoxynucleotide triphosphate (dNTP) Mix 1 μL, 5× Reaction Buffer 4 μL, RiboLock RNase Inhibitor 1 μL, RevertAid M-MuLV Reverse Transcriptase 1 μL, nuclease-free water up to 20 μL). Reaction conditions: 25°C for 5 min, 42°C for 60 min, 70°C for 5 min. Perform real-time fluorescence quantitative PCR amplification using cDNA as template. Reaction system 20 μL: 2× SYBR Green Master Mix 10 μL, upstream and downstream primers each 0.5 μL (final concentration 250 nM), cDNA template 2 μL, nuclease-free water 7 μL. Reaction conditions: 95°C pre-denaturation for 10 min; 95°C denaturation for 15 s, 60°C annealing and extension for 1 min, for 40 cycles. Using β-actin as internal control, calculate the relative expression of VEGF mRNA using the 2^-ΔΔCt^ method (Livak and Schmittgen, 2001). Primer sequences are shown in table 1. All primers were synthesized by Sangon Biotech (Shanghai) Co., Ltd.

Statistical analysis

Data were analyzed using SPSS 26.0 software and graphs were plotted using GraphPad Prism 8.0 software. All experiments were independently repeated 3 times (biological replicates), with 3 replicate wells per experiment (technical replicates). Data are expressed as mean ± standard deviation ($\bar{x} \pm s$). Normality test: Shapiro-Wilk test was used to assess the normality of data in each group. If $P > 0.05$, the data were considered to be normally distributed. Homogeneity of variance test: Levene's test was used to assess the homogeneity of variance. If $P > 0.05$, variances were considered equal. Comparison between two groups: For data conforming to normal distribution and equal variance, independent samples t-test (two-tailed) was used; for data not conforming to normal distribution or unequal variance, Mann-Whitney U test was used. Comparison among multiple groups: For data conforming to normal distribution and equal variance, one-way analysis of variance (ANOVA) was used; if the ANOVA result was statistically significant, Tukey's honestly significant difference (HSD) test was used for further pairwise comparisons (multiple comparison correction). For data not conforming to normal distribution or unequal variance, Kruskal-Wallis H test was used, followed by Dunn-Bonferroni test for pairwise comparisons. Cell phase proportions and G1/S ratio were analyzed by one-way ANOVA, with Tukey's HSD test for pairwise comparisons. Time gradient data: Comparison of protein expression at different time points was performed using repeated measures ANOVA and comparison between groups was performed using Tukey's HSD test. $P < 0.05$ was considered statistically significant.

RESULTS

Identification and characterization of exosomes

To verify the nature of the isolate, we systematically characterized EOC-Exos obtained by ultracentrifugation. TEM observation showed that EOC-Exos exhibited typical spherical or cup-shaped membranous vesicle structures (Fig. 1A). NTA results indicated that the main particle size peak of EOC-Exos was within the range of 30-150 nm, consistent with the typical size of exosomes (Fig. 1B).

Table 1: Primer sequence

Target gene		primer sequence
VEGF	upstream gene	5'-TGCCCACTGAGGAGTCCAAC-3'
	downstream gene	5'-TGGTTCCCGAAACGCTGAG-3'
β-actin	upstream gene	5'-CTGGGACGACATGGAGAAAA-3'
	downstream gene	5'-AAGGAAGGCTGGAAGAGTGC-3'。

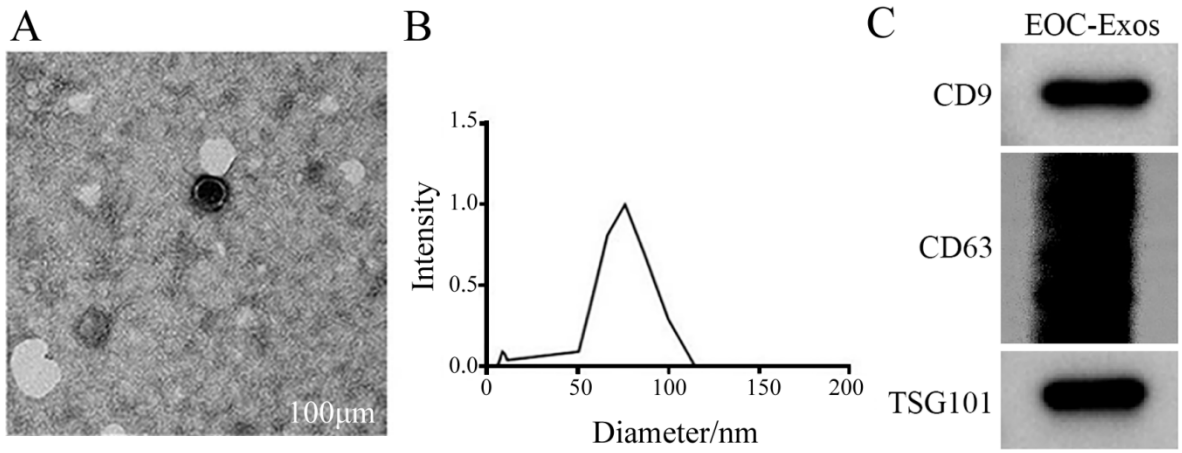

Fig. 1: Identification of EOC-derived exosomes (EOC-Exos).
(A) TEM analysis of EOC-Exos; (B) NTA of EOC-Exos particle size; (C) Western blot analysis of exosome markers CD9, CD63 and TSG101. Calnexin was used as a negative control. n=3 independent experiments (3 replicate wells per experiment).

Further detection of exosome markers by Western Blot showed that EOC-Exos were enriched for CD9, CD63 and TSG101, while the endoplasmic reticulum protein Calnexin (negative control) was negative, confirming the high purity of the isolate and excluding contamination by cell debris (Fig. 1C). These data indicate that we successfully isolated and identified highly purified EOC-Exos, which can be used for subsequent functional experiments. The above data are from 3 independent experiments (3 replicate wells per experiment).

Identification of BMSCs

To verify the stemness characteristics of the isolated cells, we identified the immunophenotype of the 3rd passage BMSCs by FCM. The results showed that the cultured cells highly expressed BMSC positive markers CD90 (99.73%), CD73 (99.29%) and CD105 (99.08%), while the expression rates of negative markers CD45 (0.87%) and CD34 (1.16%) were extremely low (Fig. 2), meeting the BMSC immunophenotypic criteria defined by the International Society for Cell & Gene Therapy (ISCT). The above data are from 3 independent experiments (3 replicate wells per experiment).

Cell cycle detected with FCM. The cell cycle in test group was block at S stage.

FCM was used to detect changes in the cell cycle distribution of BMSCs after EOC-Exos intervention. The results showed that compared with the control group, the proportion of cells in the G0/G1 phase was significantly decreased in the EOC-Exos group (59.98% ± 3.29% vs 71.41% ± 3.95%, P=0.007) and the proportion of cells in the S phase was significantly increased (27.86% ± 3.38% vs 15.35% ± 0.73%, P<0.001), while the proportion of cells in the G2/M phase did not change significantly (12.16% ± 2.51% vs 13.24% ± 3.22%, P=0.589) (Table 2, Fig. 3). The G0/G1/S ratio decreased from 4.65 ± 0.48 in the control group to 2.15 ± 0.35 in the EOC-Exos group (P<0.001), indicating that EOC-Exos intervention could promote the transition of BMSCs from G0/G1 phase to S phase and accelerate cell cycle progression. The above data are from 3 independent experiments (3 replicate wells per experiment).

Effect of EOC-Exos on the distribution of VEGF-A and total MAPK/ERK in BMSCs

Immunofluorescence staining was used to detect the localization and expression of VEGF-A and total MAPK/ERK in BMSCs. The results showed that in the control group, the fluorescence signals of VEGF-A and total MAPK/ERK were weak, with positive cell rates of 18.77% ± 1.33% and 22.07% ± 1.18%, respectively and the fluorescence signals were mainly distributed in the cytoplasm. After 24 h of EOC-Exos intervention, the green fluorescence intensity of VEGF-A and total MAPK/ERK was significantly enhanced and the positive cell rates were significantly increased (P<0.001 vs control group) (Fig. 4A). The fluorescence signals were still mainly distributed

in the cytoplasmic region and DAPI staining of the nucleus showed no obvious abnormalities. Image J software was used for quantitative analysis of fluorescence intensity, standardizing the control group fluorescence intensity to 1.0. The results showed that the relative fluorescence intensity of VEGF-A in the EOC-Exos group was significantly higher than that in the control group (P<0.001) (Fig. 4B); the relative fluorescence intensity of total MAPK/ERK was significantly higher than that in the control group (P<0.001) (Fig. 4C). These results indicate that EOC-Exos can significantly promote the expression of VEGF-A and total MAPK/ERK proteins in BMSCs. The above data are from 3 independent experiments, analyzing 10 random fields per group.

Effect of EOC-Exos on VEGF-A and total ERK protein expression in BMSCs

Western Blot was used to detect the protein expression levels of VEGF-A and total ERK in BMSCs at different time points after EOC-Exos intervention. The results showed that compared with the control group, the VEGF-A protein expression level in the EOC-Exos group gradually increased over time and was significantly higher than that in the control group at all time points, with statistical significance (P<0.05). The total ERK protein expression level showed no significant difference among the groups (P>0.05) (Fig. 5). This result provides an important control for the subsequent observation of changes in ERK phosphorylation (see Fig. 7), indicating that the change in p-ERK is not caused by a change in total protein amount. The above data are from 3 independent experiments (3 replicate wells per experiment).

Effect of EOC-Exos on ERK phosphorylation in BMSCs and verification of ERK inhibitor inhibition

To verify whether EOC-Exos activate the ERK signaling pathway, we detected the expression level of p-ERK at different time points. The results showed that compared with the control group, the p-ERK expression level in the EOC-Exos group gradually increased over time and was significantly higher than that in the control group at all time points (P<0.05). Expressed as the p-ERK/total ERK ratio, the ratios at each time point in the EOC-Exos group were significantly higher than those in the control group (P<0.001) (Fig. 6A). These results indicate that EOC-Exos can induce the phosphorylation and activation of the ERK pathway in BMSCs. To verify the effectiveness of the ERK inhibitor U0126, we detected the p-ERK/total ERK expression level in the EOC-Exos + ERK inhibitor group. The results showed that compared with the EOC-Exos group (72 h), the p-ERK/total ERK ratio in the EOC-Exos + ERK inhibitor group was significantly reduced (P<0.001), while there was no significant difference between the DMSO solvent control group and the control group (P>0.05) (Figs. 6B-C). These results indicate that U0126 effectively inhibited the ERK pathway activation induced by EOC-Exos, providing a reliable pharmacological tool for subsequent functional experiments. The above data are from 3 independent experiments (3 replicate wells per experiment).

Effect of EOC-Exos on VEGF protein secretion and mRNA expression in BMSCs

ELISA and real-time quantitative PCR were used to detect VEGF protein secretion levels and mRNA expression levels in BMSCs of each group, respectively. ELISA results showed (Fig. 7A) that the VEGF concentration in the culture supernatant of BMSCs in the control group was 156.3 ± 18.7 pg/mL. Compared with the control group, the VEGF concentration in the EOC-Exos group was significantly increased (P<0.001). Compared with the EOC-Exos group, the VEGF concentration in the EOC-Exos + U0126 group was significantly decreased (P=0.002 vs EOC-Exos group), but still higher than that in the control group (P=0.023 vs control group). The VEGF concentration in the DMSO solvent control group showed no significant difference compared with the control group (P=0.892). Real-time quantitative PCR analysis results showed (Fig. 7B) that compared with the control group, the relative expression of VEGF mRNA in the EOC-Exos group was significantly increased (P<0.001). Compared with the EOC-Exos group, the relative expression of VEGF mRNA in the EOC-Exos + U0126 group was significantly decreased (P=0.004 vs EOC-Exos group), but still higher than that in the control group (P=0.018 vs control group). The relative expression of VEGF mRNA in the DMSO solvent control group showed no significant difference compared with the control group (P=0.895). These results indicate that EOC-Exos can upregulate VEGF expression at the transcriptional level and promote VEGF protein secretion and this process is regulated by the ERK pathway. The above data are from 3 independent experiments (3 replicate wells per experiment).

Effect of ERK inhibitor on EOC-Exos-induced VEGF expression and cell cycle

To verify the necessity of the ERK pathway in EOC-Exos regulation of BMSC function, we pretreated BMSCs with the ERK-specific inhibitor U0126 and then detected VEGF expression and cell cycle changes. Western Blot results showed that compared with the EOC-Exos group, the VEGF protein expression level in the EOC-Exos + ERK inhibitor group was significantly decreased (P<0.01) (Fig. 8A). ELISA results showed that the VEGF concentration in the supernatant of the EOC-Exos + ERK inhibitor group was significantly lower than that in the EOC-Exos group (P<0.01) (Fig. 8B). FCM results showed that compared with the EOC-Exos group, the proportion of cells in S phase in the EOC-Exos + ERK inhibitor group was significantly decreased (P<0.01) and the proportion of cells in G0/G1 phase was significantly increased (P<0.05) (Fig. 8C) (Table 3).

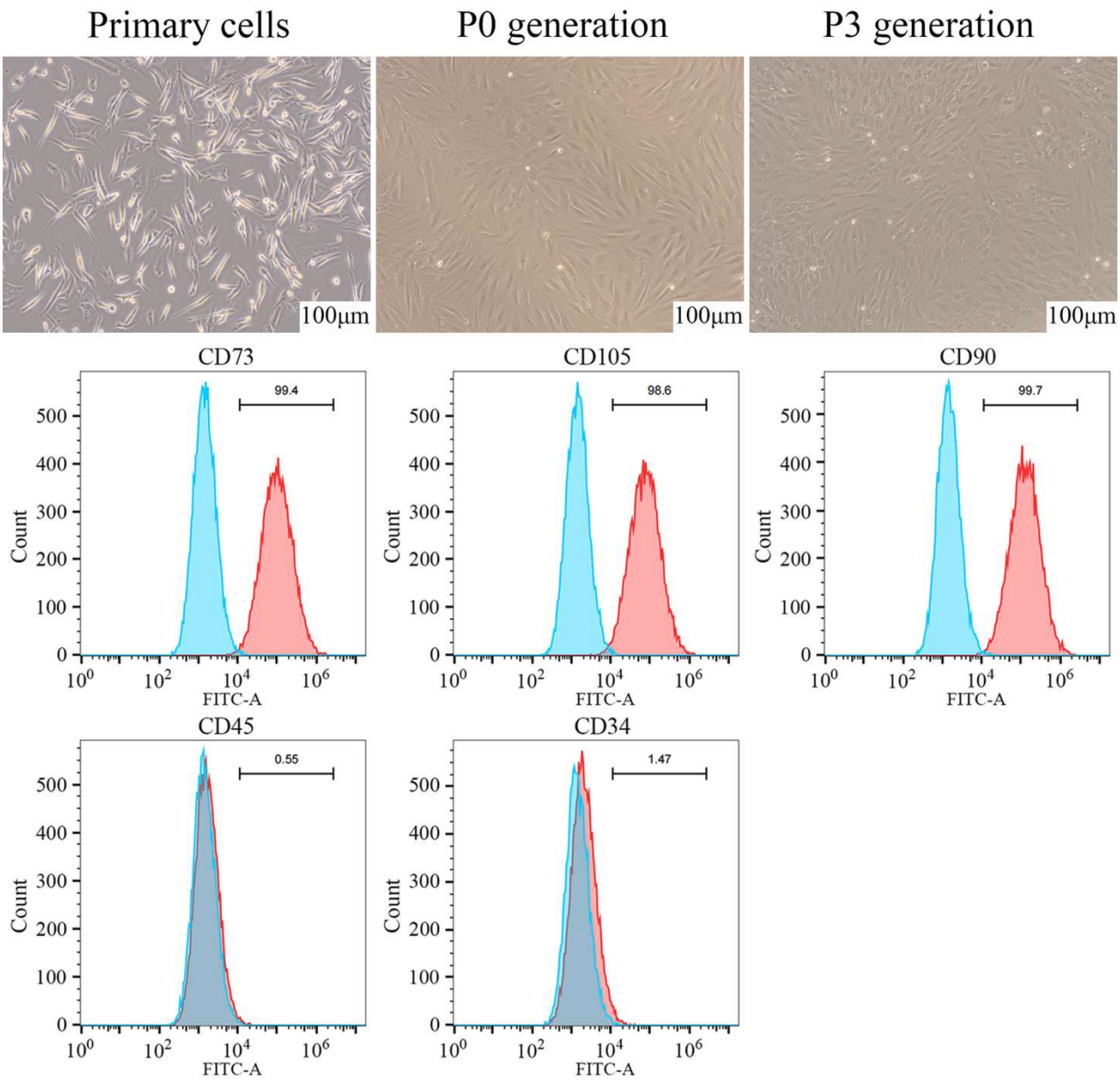

Fig. 2: Identification of surface markers of BMSCs by FCM.
Note: n=3 independent experiments (3 replicate wells per experiment).

Table 2: Action of exosome derived from EOC on distribution of BMSCs cells ($\bar{x} \pm s$, percent).

Group	G1 (%)	S (%)	G2 (%)	G1/S (%)
control group	71.41±3.95	15.35±0.73	13.24±3.22	4.65±0.48
EOC-Exos group	59.98±3.29**	27.86±3.38***	12.16±2.51	2.15±0.35***
F	3.851	6.266	0.458	7.289
P	0.018	0.003	0.671	0.002

Note: Compared with the control group, **P<0.01, ***P<0.001; n=3 independent experiments. The sum of the proportions of G0/G1, S, and G2/M phases is approximately 100%. Statistical method: one-way ANOVA, Tukey HSD multiple comparison test.

Table 3: The effect of ERK inhibitors on the cell cycle distribution of BMSCs induced by EOC-Exos ($\bar{x} \pm s$, n=3)

Group	G0/G1 (%)	S (%)	G2/M (%)	G0/G1/S (%)
Control group	71.41±3.95	15.35±0.73	13.24±3.22	4.65±0.48
DMSO group	70.82±3.87	15.62±0.81	13.56±3.06	4.53±0.45
EOC-Exos group	59.98±3.29**	27.86±3.38***	12.16±2.51	2.15±0.35***
EOC-Exos+U0126 group	68.15±4.08#	18.62±2.14##	13.23±2.67	3.66±0.41##
t	8.324	18.562	0.412	15.876
P	0.002	<0.001	0.745	<0.001

Note: Compared with the control group, **P < 0.01, ***P < 0.001; compared with the EOC-Exos group, #P < 0.05, ##P < 0.01. n = 3 independent experiments. The sum of the proportions in each period is approximately 100%. Statistical method: one-way analysis of variance, TukeyHSD multiple comparison test.

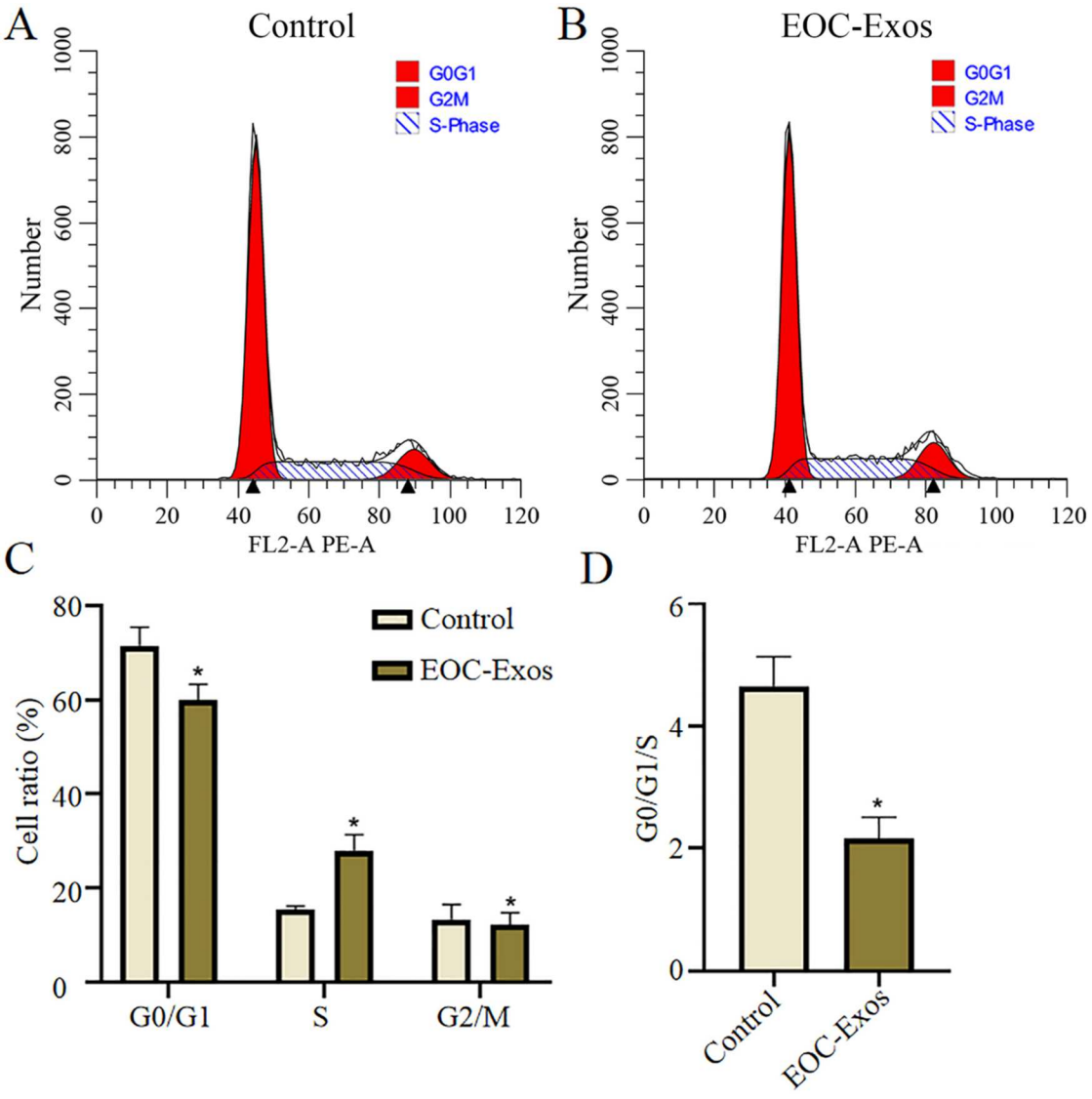

Fig. 3: Effect of EOC-Exos on the cell cycle of BMSCs.
(A-B) Representative images of cell cycle distribution in BMSCs detected by FCM. (A) Control group; (B) EOC-Exos group. G0/G1: Quiescent phase/G1 phase; S: DNA synthesis phase; G2/M: G2 phase/Mitosis phase. (C) Quantitative analysis of the proportion of cells in G0/G1, S, and G2/M phases in each group. (D) Quantitative analysis of the G0/G1/S ratio. Data are expressed as $\bar{x} \pm s$, n=3 independent experiments (3 replicate wells per experiment). *P<0.05 vs control group. Statistical method: one-way ANOVA, Tukey's HSD multiple comparison test.

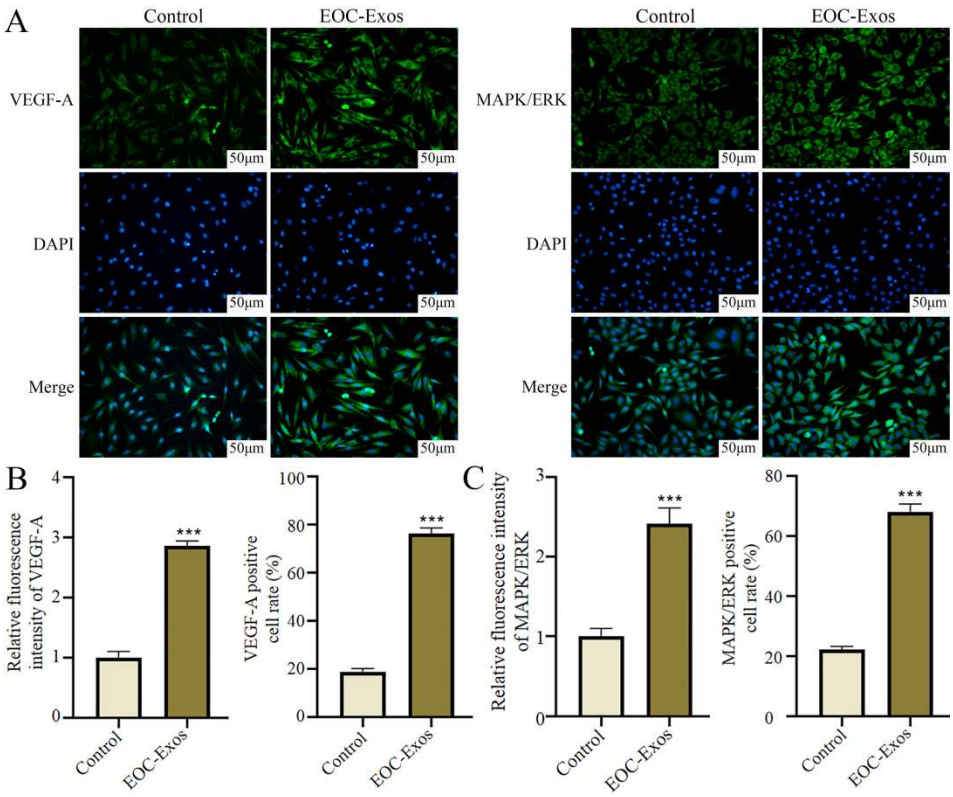

Fig. 4: Immunofluorescence staining detecting the distribution of VEGF-A and total MAPK/ERK in BMSCs (A) Representative immunofluorescence images showing the expression and distribution of VEGF-A (green) and total MAPK/ERK (green) in BMSCs. Nuclei were counterstained with DAPI (blue). Scale bar = 50 μm; (B) Quantitative analysis of VEGF-A fluorescence intensity. Mean fluorescence intensity from 10 random fields per group was analyzed using Image J software and normalized to the control group; (C) Quantitative analysis of total MAPK/ERK fluorescence intensity. ***P<0.001 vs control group. Data are expressed as $\bar{x} \pm s$, n=3 independent experiments (10 fields analyzed per group per experiment). Statistical method: independent samples t-test.

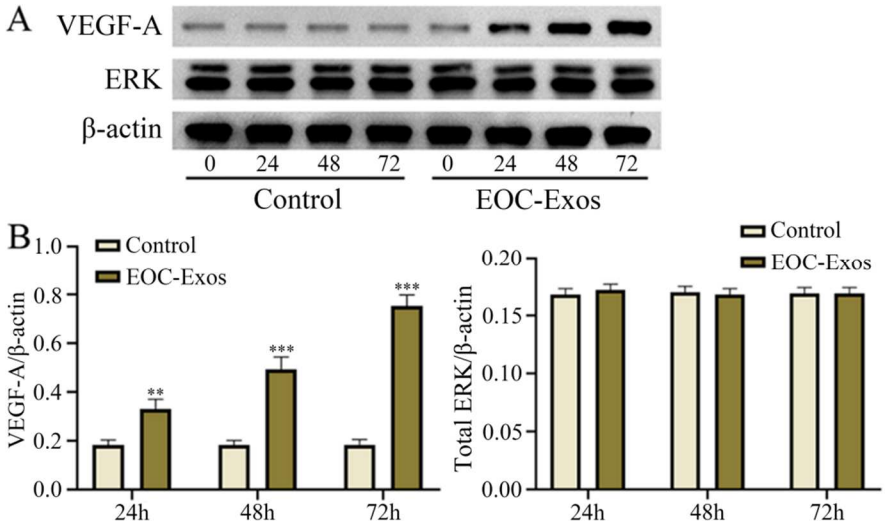

Fig. 5: Effect of EOC-Exos on VEGF-A and total ERK protein expression in BMSCs.
(A) Representative Western blot bands showing VEGF-A, total ERK, and β-actin protein expression in BMSCs at different time points. (B) Quantitative analysis of relative VEGF-A and total ERK protein expression. Normalized to β-actin and calibrated to control 24 h. *P<0.05 vs control group. Data are expressed as $\bar{x} \pm s$, n=3 independent experiments. Statistical method: one-way ANOVA, Tukey's HSD multiple comparison test.

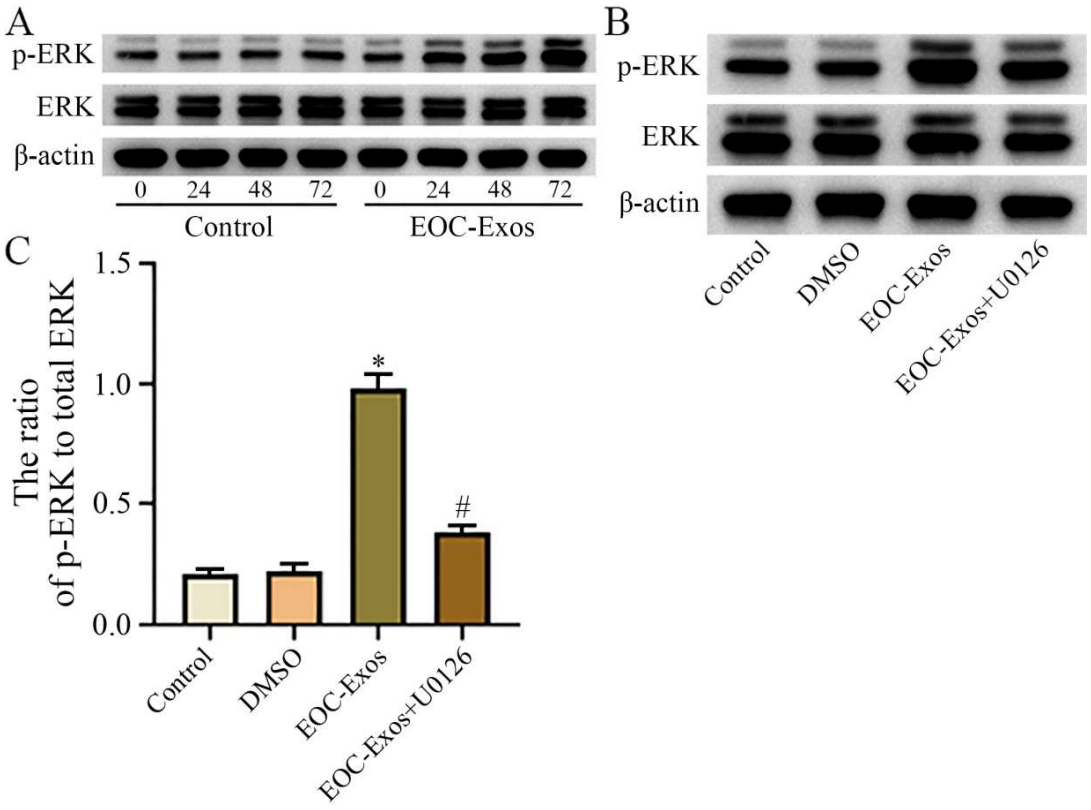

Fig. 6: Effect of EOC-Exos on ERK phosphorylation in BMSCs and verification of ERK inhibitor inhibition.
(A) Representative bands of p-ERK and the ratio of p-ERK to total ERK protein expression in BMSCs at different time points were detected by Western Blot. (B) Representative band of the protein expression of p-ERK/total ERK was detected by Western Blot. (C) Quantitative analysis of p-ERK/total ERK (inhibitor validation). Compared with the control group, *P < 0.001; compared with the EOC-Exos group, #P < 0.001. Data are presented as $\bar{x}$ ± s, n = 3 independent experiments. Statistical methods: One-way analysis of variance, Tukey HSD multiple comparison test.

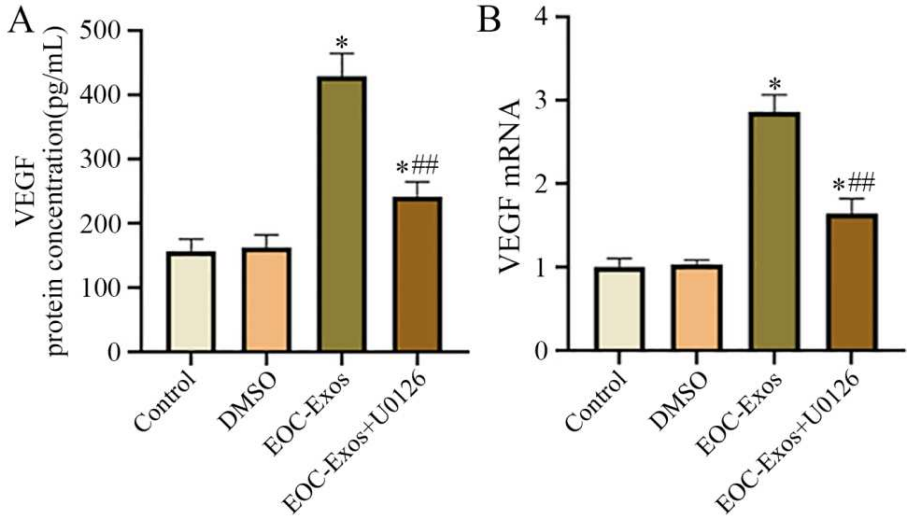

Fig. 7: Detection of VEGF expression in BMSCs by ELISA and RT-PCR.
(A) ELISA detection of VEGF protein content in the culture supernatant of BMSCs in each group. (B) Real-time quantitative PCR detection of relative VEGF mRNA expression in BMSCs of each group. Calculated using the 2^-ΔΔCt^ method, with β-actin as internal control, normalized to the control group. *P<0.05 vs control group; #P<0.05 vs EOC-Exos group. Data are expressed as $\bar{x}$ ± s, n=3 independent experiments (3 replicate wells per experiment). Statistical method: one-way ANOVA, Tukey's HSD multiple comparison test.

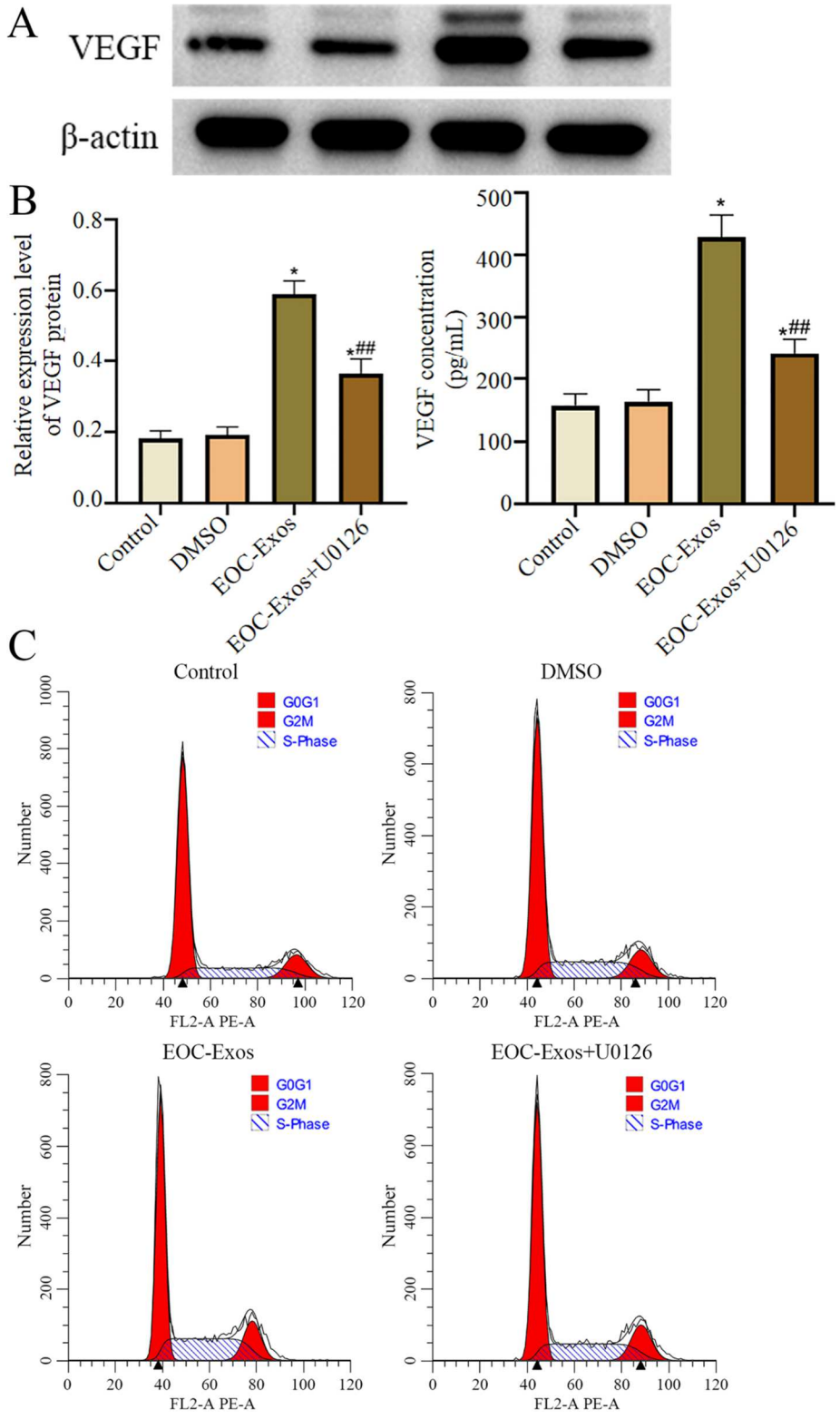

Fig. 8: Effect of ERK inhibitor on EOC-Exos-induced VEGF expression and cell cycle.
(A) Representative Western blot bands and quantitative analysis of VEGF protein expression in BMSCs of each group; (B) ELISA detection of VEGF concentration in the culture supernatant of each group; (C) Representative images of cell cycle distribution in each group detected by FCM. ***P<0.001 vs control group; #P<0.05, ##P<0.01 vs EOC-Exos group. Data are expressed as $\bar{x} \pm s$, n=3 independent experiments (3 replicate wells per experiment). Statistical method: one-way ANOVA, Tukey's HSD multiple comparison test.

These results indicate that inhibiting the ERK pathway can significantly attenuate the EOC-Exos-induced upregulation of VEGF expression and acceleration of cell cycle progression, confirming that the ERK pathway plays a key role in EOC-Exos regulation of BMSC function. The above data are from 3 independent experiments (3 replicate wells per experiment).

DISCUSSION

VEGF participates in the formation of new blood vessels during tumor cell growth and its expression in the microenvironment partly originates from the autocrine mechanism of tumor cells (Boichuk *et al*., 2024). VEGF regulates the biological characteristics of cells by activating downstream signaling pathways (Elebiyo *et al*., 2022). This study aimed to investigate the promoting effect of EOC-derived exosomes on BMSCs and their autocrine effect in the microenvironment through activation of the VEGF-A/MAPK/ERK signaling pathway, providing experimental evidence for the study of tumor-stroma interactions.

First, we identified the growth state and surface markers of BMSCs. FCM results showed that the third-passage BMSCs highly expressed the mesenchymal stem cell positive markers CD90, CD73 and CD105, while the expression rates of the negative markers CD45 and CD34 were extremely low, meeting the BMSC immunophenotypic criteria defined by the ISCT, indicating that the cells were in good condition and suitable for subsequent functional experiments. Regarding the effect of EOC-Exos on the BMSC cell cycle, FCM results showed that the proportion of BMSCs in the G0/G1 phase in the EOC-Exos intervention group was significantly lower than that in the control group and the proportion in the S phase was significantly higher than that in the control group, while the proportion in the G2/M phase did not change significantly. This indicates that EOC-Exos can promote the transition of BMSCs from G0/G1 phase to S phase, accelerate cell cycle progression and thus promote the proliferation of BMSCs. To explore the molecular mechanism by which EOC-Exos regulate the BMSC cell cycle, we detected the activation status of the VEGF-A/MAPK/ERK pathway. Western Blot results showed that compared with the control group, the VEGF-A protein expression level in BMSCs increased in a time-dependent manner after EOC-Exos intervention. The total ERK protein expression level showed no significant difference among the groups, providing an important control for subsequent p-ERK detection. Further detection of ERK phosphorylation levels showed that the p-ERK expression level in the EOC-Exos group gradually increased over time and was significantly higher than that in the control group. The p-ERK/total ERK ratio at each time point in the EOC-Exos group was also significantly higher than that in the control group. Immunofluorescence staining further confirmed that after EOC-Exos intervention, the fluorescence intensity of VEGF-A and total MAPK/ERK in BMSCs was significantly enhanced. This indicates that EOC-Exos can activate the VEGF-A/MAPK/ERK signaling pathway in BMSCs and this activation effect is time-dependent.

Tumor-derived exosomes can regulate the function of recipient cells by carrying specific mRNAs, miRNAs, or proteins (Luongo *et al*., 2024). Therefore, it is speculated that EOC-Exos may carry VEGF mRNA or related regulatory molecules such as miR-210, miR-21, etc. After entering BMSCs through membrane fusion or endocytosis (Zhou *et al*., 2023), they release their contents, thereby activating downstream transcription factors, initiating the autocrine expression of VEGF (Zhang *et al*., 2022) and enhancing the activation of the MAPK/ERK pathway through a positive feedback mechanism (Feng *et al*., 2022). EOC-Exos can be effectively taken up by BMSCs and significantly upregulate the protein expression levels of VEGF-A and MAPK/ERK within the cells (Huang *et al*., 2024), rapidly intervening in the cell cycle regulation mechanism of recipient cells and exerting a pro-proliferative effect (Chung *et al*., 2024; Eguchi *et al*., 2022). However, since this study did not design experiments for exosome uptake and identification of exosome contents, the above speculations need to be verified in subsequent studies. This study observed that after exosome intervention, the VEGF content in the BMSC supernatant significantly increased and the VEGF mRNA expression level was significantly higher than that in the control group and the ERK inhibitor group, suggesting that after being activated, BMSCs not only enhance their autocrine function but may also package VEGF or other signaling molecules into secondary exosomes, thereby affecting other surrounding cells. This is mainly because BMSC-derived secondary exosomes carry specific membrane proteins on their surface and tend to be taken up by specific cells in the tumor microenvironment, thereby ensuring that signaling molecules mainly act on cell populations requiring regulation, improving the efficiency and specificity of signal transmission (Zhang *et al*., 2024), thus playing a role in regulating other surrounding cells; at the same time, after EOC-Exos activate the VEGF-A/MAPK/ERK pathway in BMSCs, the VEGF autocrine capacity of BMSCs is significantly enhanced, which may then act on vascular endothelial cells through paracrine signaling, promoting new blood vessel formation (Fei *et al*., 2025), thereby affecting other surrounding cells.

This study systematically verified the mechanism by which exosomes regulate VEGF expression in BMSCs through the ERK pathway in the context of EOC, providing time-gradient data support; confirmed the necessity of the ERK pathway through inhibitor experiments, rather than just correlation; verified the regulatory effect of EOC-Exos on VEGF at both protein and transcriptional levels; and linked

cell cycle changes with pathway activation, forming a relatively complete chain of evidence. However, this study did not identify the contents of exosomes or secondary exosomes, lacked research on receptor interaction mechanisms, functional angiogenesis experiments and in vivo experimental validation. Subsequent studies need to be improved from the above aspects to more comprehensively elucidate the mechanism of EOC-Exos in the ovarian cancer tumor microenvironment.

CONCLUSION

In conclusion, this study systematically verified that EOC-Exos can upregulate VEGF expression in BMSCs at the transcriptional level, promote VEGF protein secretion and accelerate cell cycle progression by activating the MAPK/ERK pathway. ERK inhibitors can significantly attenuate the above effects, confirming the necessity of this pathway. As a mechanistic study, this research provides reliable experimental evidence for understanding tumor-stroma interactions in the EOC microenvironment and lays a solid foundation for future exploration of exosome contents, receptor interactions and angiogenic functions.

Acknowledgments
No funding support.

Authors' contribution
Shuhan Lv: responsible for research design, experimental operation, data analysis and manuscript writing.
Yong Liang: Supervision, Project Administration, Writing – Review & Editing.
Chengbin Wang: Conceptualization, Supervision, Funding acquisition, Writing – review & editing.

Funding
There was no funding.

Data availability statement
The datasets generated during and/or analysed during the current study are available from the corresponding author on reasonable request.

Ethical approval
This study was approved by the ethics committee of Guizhou University of Traditional Chinese Medicine (NO.GZ-ZYD2025298).

Conflict of interest
This research was conducted in the absence of any commercial or financial relationships that could be construed as a potential conflict of interest.

REFERENCES

Boichuk S, Dunaev P, Galembikova A and Valeeva E (2024). Fibroblast growth factor 2 (FGF2) activates vascular endothelial growth factor (VEGF) signaling in gastrointestinal stromal tumors (GIST): an autocrine mechanism contributing to imatinib mesylate (IM) resistance. *Cancers*., **16**(17): 3103.

Chen L, Xie X, Wang T, Xu L, Zhai Z, Wu H, Deng L, Lu Q, Chen Z, Yang X, Lu H, Chen YG and Luo S (2023). ARL13B promotes angiogenesis and glioma growth by activating VEGFA-VEGFR2 signaling. *Neuro Oncol*., **25**(5): 871-885.

Chung JY, Lee W, Lee OW, Ylaya K, Nambiar D, Sheehan-Klenk J, Fayn S, Hewitt SM, Choyke PL and Escorcia FE (2024). Glypican-3 deficiency in liver cancer upregulates MAPK/ERK pathway but decreases cell proliferation. *Am J Cancer Res*., **14**(7): 3348-3371.

Doppelt-Flikshtain O, Younis A, Tamari T, Ginesin O, Shentzer-Kutiel T, Nikomarov D, Bar-Sela G, Coyac BR, Assaraf YG and Zigdon-Giladi H (2023). Endothelial progenitor cells promote osteosarcoma progression and Invasiveness via AKT/PI3K Signaling. *Cancers*, **15**(6): 1818.

Eguchi R, Kawabe JI and Wakabayashi I (2022). VEGF-Independent angiogenic factors: Beyond VEGF/VEGFR2 signaling. *J Vasc Res*., **59**(2): 78-89.

Elebiyo TC, Rotimi D, Evbuomwan IO, Maimako RF, Iyobhebhe M, Ojo OA, Oluba OM and Adeyemi OS (2022). Reassessing vascular endothelial growth factor (VEGF) in anti-angiogenic cancer therapy., *Cancer Treat Res Commun*, **32**: 100620.

Elieh-Ali-Komi D, Shafaghat F, Alipoor SD, Kazemi T, Atiakshin D, Pyatilova P and Maurer M (2025). Immunomodulatory significance of mast cell exosomes (MC-EXOs) in immune response coordination. *Clin Rev Allergy Immunol*., **68**(1), 20.

Fei J and Guo Y (2025). MAPK/ERK Signaling in Tumorigenesis: Mechanisms of growth, invasion and angiogenesis. *EXCLI J*., **24**: 854-879.

Feng Y, Li X, Wang J, Huang X, Meng L and Huang J (2022). Pyruvate kinase M2 (PKM2) improve symptoms of post-ischemic stroke depression by activating VEGF to mediate the MAPK/ERK pathway. *Brain Behav*., **12**(1): e2450.

Gangadaran P, Madhyastha H, Madhyastha R, Rajendran R L, Nakajima Y, Watanabe N, Velikkakath AKG, Hong CM, Gopi RV, Muthukalianan GK, Valsala Gopalakrishnan A, Jeyaraman M and Ahn BC (2023). The emerging role of exosomes in innate immunity, diagnosis and therapy. *Front Immunol*., **13**: 1085057.

Huang S, Long Y, Gao Y, Lin W, Wang L, Jiang J, Yuan X, Chen Y, Zhang P and Chu Q (2024). Combined inhibition of MET and VEGF enhances therapeutic efficacy of EGFR TKIs in EGFR-mutant non-small cell lung cancer with concomitant aberrant MET activation. *Exp Hematol Oncol*., **13**(1): 97.

Iqbal MJ, Kabee, A, Abbas Z, Siddiqui HA, Calina D, Sharifi-Rad J and Cho WC (2024). Interplay of oxidative stress, cellular communication and signaling pathways in cancer. *Cell Commun Signal.,* CCS, **22**(1):

7.

Kimura M, Miyahara K, Yamasaki M and Uchida N (2022). Comparison of vascular endothelial growth factor/vascular endothelial growth factor receptor 2 expression and its relationship to tumor cell proliferation in canine epithelial and mesenchymal tumors. *J Vet Med Sci*., **84**(1): 133-141.

Lei X, Li Z, Huang M, Huang L, Huang Y, Lv S, Zhang W, Chen Z, Ke Y, Li S, Chen J, Yang X, Deng Q, Liu J and Yu X (2024). Gli1-mediated tumor cell-derived bFGF promotes tumor angiogenesis and pericyte coverage in non-small cell lung cancer. *J Exp Clin Cancer Res*., **43**(1): 83.

Leong SP, Naxerova K, Keller L, Pantel K and Witte M (2022). Molecular mechanisms of cancer metastasis via the lymphatic versus the blood vessels. *Clin Exp Metastasis*., **39**(1): 159-179.

Liang PI, Wei YC, Chen HD, Ma YC, Ke HL, Chien CC and Chuang HW (2024). TGFB1I1 promotes cell proliferation and migration in urothelial carcinoma. *Kaohsiung J Med Sci*., **40**(3): 269-279.

Liu J, Gao J, Liang Z, Gao C, Niu, Q, Wu F and Zhang L (2022). Mesenchymal stem cells and their microenvironment. *Stem Cell Res Ther*., **13**(1): 429.

Livak KJ and Schmittgen TD (2001). Analysis of relative gene expression data using real-time quantitative PCR and the 2(-Delta Delta C(T)) Method. *Methods,* **25**(4): 402-408.

Luongo M, Laurenziello P, Cesta G, Bochicchio AM, Omer LC, Falco G, Milone MR, Cibarelli F, Russi S and Laurino S (2024). The molecular conversations of sarcomas: Exosomal non-coding RNAs in tumor's biology and their translational prospects. *Mol Cancer*., **23**(1): 172.

Murase Y, Yokogawa R, Yabuta Y, Nagano M, Katou Y, Mizuyama M, Kitamura A, Puangsricharoen P, Yamashiro C, Hu B, Mizuta K, Tsujimura T, Yamamoto T, Ogata K, Ishihama Y and Saitou M (2024). *In-vitro* reconstitution of epigenetic reprogramming in the human germ line. *Nature*., **631**(8019), 170-178.

Wu M, Guo Z, Xie Y, Liu H, Chen H, Lin X, Chen R, Shen A and Peng J (2025). Mechanism of trifolin in attenuating hypertension-induced renal cell apoptosis via modulation of the MAPK signaling pathway. *Sichuan Da Xue Xue Bao Yi Xue Ban*., **56**(5): 1273-1280.

Yang Z, Wang T, Wu D, Min Z, Tan J and Yu B (2020). RNA N6-methyladenosine reader IGF2BP3 regulates cell cycle and angiogenesis in colon cancer. *J Exp Clin Cancer Res*, **39**(1): 203.

Zhang Q, Li T, Li Z, Lu J, Wu X, Gao F and Sun W (2022). Autocrine activity of extracellular vesicles induced by icariin and its effectiveness in glucocorticoid-induced injury of bone microvascular endothelial cells. *Cells*., **11**(12): 1921.

Zhang WY, Wen L, Du L, Liu TT, Sun Y, Chen YZ, Lu YX, Cheng XC, Sun HY, Xiao FJ and Wang LS (2024). S-RBD-modified and miR-486-5p-engineered exosomes derived from mesenchymal stem cells suppress ferroptosis and alleviate radiation-induced lung injury and long-term pulmonary fibrosis. *J Nanobiotechnology.*, **22**(1): 662.

Zhou YK, Han CS, Zhu ZL, Chen P, Wang YM, Lin S, Chen LJ, Zhuang ZM, Zhou YH and Yang RL (2023). M2 exosomes modified by hydrogen sulfide promoted bone regeneration by moesin mediated endocytosis. *Bioact Mater*., **31**: 192-205.